1992-09-01

Heterogeneity of Intergranular Damage in Copper Crept in Plane-Strain Tension

Brent L. Adams
b_l_adams@byu.edu

David P. Field

Original Publication Citation

Metall. Trans., 23A, 2515-26, (1992).

HETEROGENEITY OF INTERGRANULAR DAMAGE IN COPPER CREPT IN PLANE-STRAIN TENSION

David P. Field and Brent L. Adams

Abstract

An interface damage function (IDF), which statistically describes the area fraction of interface damage as a function of up to eight parameters defining crystallite interfaces, was determined for commercial purity copper specimens crept in plane strain tension. The IDF was determined from stereological parameters measured on plane sections cut through damaged specimens. The eight-dimensional space of the function was investigated by analyzing two-dimensional projections of the complete domain. Certain "special" interfaces were observed to damage preferentially. A low planar density of atoms near crystallite interfaces apparently increased the propensity for the occurrence of damage. Other microstructural mechanisms contributing to the observed heterogeneous distribution of damage are also considered.

1. Introduction

Intergranular creep damage is a commonly observed phenomenon occurring in various engineering materials subjected to extreme conditions. The nucleation, growth and coalescence of voids on grain boundaries under certain conditions leads to fracture at very low strains. This brittle behavior has been observed in nickel [1], brass [2], copper [3], and stainless-steel [4], as well as in creep-resistant superalloys [5]. Creep damage is generally observed to occur heterogeneously throughout the microstructure except under certain laboratory conditions where voids are artificially distributed uniformly to study growth behavior. Uniform diffusional void growth has been studied in detail since the classical works of Hull and Rimmer [6] and Speight and Harris [7] in the 1950's. The "constrained cavitation" ideas of Dyson [8] and Rice [9], among others, in the last couple of decades have introduced into models of void growth the fact that damage does not occur uniformly on all boundaries. In these models, however, it is generally assumed that constrained "clusters" of voids are distributed uniformly throughout the microstructure. This assumption is contrary to common experimental observation.

In recent years, technological advances have made it possible to focus attention on local interfacial characteristics in an attempt to identify the types of interfaces which are preferentially damaged under given conditions. It has been suggested that low Σ coincident site lattice (CSL) boundaries are generally damage resistant [10,11]. Other studies tend to contradict this conclusion and indicate that additional information is required in the classification of damage resistant, and damage prone, interfaces [12,13].

A powerful tool, known as an interface damage function (IDF), has been developed for the measurement of intergranular damage [14,15]. This function, which gives the area fraction of damaged interface as a function of grain boundary structure, has been measured in copper specimens crept in uniaxial tension. In the present study the IDF is employed to investigate damage in copper specimens crept under plane-strain tensile loading conditions. This stress-state commonly occurs in sheet and plate structural components [cf. 16], and the resulting local stress gradients near crystallite interfaces differ significantly from those created by imposed uniaxial tension.

In the following discussion the analytical technique utilized in calculating the IDF has been significantly altered from that used in the previous analyses as the technique here employed was determined to yield more accurate information with less experimental effort. A comparison of various methods of utilizing stereological measures in determining the three-dimensional structure distribution function from plane sections is the subject of a separate companion paper [17].

The IDF measurements presented in this paper describe the damage distribution over a domain comprised of up to three independent orientation parameters which define the local geometric structure of crystallite interfaces. These parameters include the orientation of each crystallite lattice as well as that of the interface normal. Consider a laboratory coordinate frame, K_L, with mutually orthogonal axes parallel to the rolling (RD), transverse (TD), and normal (ND) directions of the plate from which the specimens were cut. The active transformation of K_L to the coordinate frame of a "reference" crystallite, K_A (having axes parallel to the <100> directions of the lattice), is here represented by Q. The Euler angles $(\varphi_1,\Phi,\varphi_2)$, as given by Bunge [18], will be used to parameterize the rotation, $Q=Q(\varphi_1,\Phi,\varphi_2)$. Specifically, for axes $\mathbf{e}_L^1$, $\mathbf{e}_L^2$, $\mathbf{e}_L^3$, defining K_L, the Euler angles describe rigid body rotations of φ_2 about $\mathbf{e}_L^3$ followed by a rotation of Φ about $\mathbf{e}_L^1$, and finally a rotation of φ_1 about $\mathbf{e}_L^3$. It should be noted that the matrix of direction cosines which transforms K_L into K_A is given by g $(= Q^{-1} = Q^T)$.

Consider a grain which neighbors the reference grain described above and defines a coordinate frame K_B. The orientation of the neighboring grain relative to the coordinate

frame of the reference grain is given by the misorientation Q^c which actively transforms K_A into K_B. Q^c will be specified by the Euler angles (α,β,γ) in this paper [cf. 17]. The orientation of the normal to the crystallite interface, **n**, is given in K_A by the polar and azimuthal angles, χ and η. The parameters Q^c and **n** constitute the five "macroscopic" degrees of freedom necessary to describe a crystallite interface. However, when a stress is applied with respect to K_L, it is necessary to include Q in the description of the grain boundary. It is also convenient to give **n** with respect to K_L. The interface normal orientation with respect to the laboratory coordinate frame, $\mathbf{n}^L$, is given simply by $\mathbf{n}^L = Q\cdot\mathbf{n}$. Note also that the orientation of the neighboring crystallite, Q_B, is equivalent to $Q\cdot Q^c$. Therefore, a geometrical description of grain boundaries under a given stress state requires up to eight independent parameters comprising Q, Q^c, Q_B, $\mathbf{n}^L$, and **n** in various combinations (e.g. (**n**, Q^c) or (Q, $\mathbf{n}^L$,Q_B)).

2. Stereological and Numerical Procedures

The stereological measure $L_A(Q_A, \omega, Q_B \mid \mathbf{p})$ was employed in determining the probability density function $f(Q_A, \mathbf{n}^L, Q_B)$. $f(Q_A, \mathbf{n}^L, Q_B)$ is understood to be that function which, when integrated over its entire domain yields S_V, the total surface area of crystallite interface per unit volume. $L_A(Q_A, \omega, Q_B \mid \mathbf{p})$ is defined as the line length of grain boundary, having orientation ω and separating crystallites of orientations Q_A and Q_B, per unit area of a section plane with normal orientation given by **p**. $f(Q_A,\mathbf{n}^L,Q_B)$ is the surface area of crystallite interface, having normal orientation $\mathbf{n}^L$ and separating crystallites with orientations Q_A and Q_B, per unit volume). Each of these functions can be expressed by an infinite Fourier series

$$ {}^{j}L_A(Q_A, \omega, Q_B) = \sum_{t=-\infty}^{\infty} \sum_{l=0}^{\infty} \sum_{\mu=1}^{M(l)} \sum_{n=-l}^{l} \sum_{l'=0}^{\infty} \sum_{\mu'=1}^{M(l')} \sum_{n=-l'}^{l'} {}^{l'\mu'n'}_{l\mu n}L^{j}_{t}\, e^{it\omega}\, \dot{T}^{\mu n}_{l}(Q_A)\, \dot{T}^{\mu' n'}_{l'}(Q_B) \tag{1} $$

$$ f(Q_A, \mathbf{n}^L, Q_B) = \sum_{r=0}^{\infty} \sum_{p=-r}^{r} \sum_{l=0}^{\infty} \sum_{\mu=1}^{M(l)} \sum_{n=-l}^{l} \sum_{l'=0}^{\infty} \sum_{\mu'=1}^{M(l')} \sum_{n=-l'}^{l'} {}^{l'\mu'n'}_{l\mu n}S^{p}_{r}\, K^{p}_{r}(\mathbf{n}^L)\, \dot{T}^{\mu n}_{l}(Q_A)\, \dot{T}^{\mu' n'}_{l'}(Q_B) \tag{2} $$

where the superscript j indicates the jth section plane having normal orientation $^{j}\mathbf{p}$ (written for the sake of brevity). In the above equations, $^{l'\mu'n'}_{l\mu n}L^{j}_{t}$ and $^{l'\mu'n'}_{l\mu n}S^{p}_{r}$ are constant coefficients defining the given functions, $K^{p}_{r}(\mathbf{n}^{L})$ are the spherical surface harmonics, and $\dot{T}^{\mu n}_{l}(Q_A)$, are the generalized spherical harmonic functions exhibiting cubic crystal symmetry and no particular sample symmetry [cf. 18].

The $^{l'\mu'n'}_{l\mu n}L^{j}_{t}$ coefficients are determined directly from observations of grain boundary morphology apparent on the jth section plane. A simple extension of previous results [17] yields the values of these coefficients

$$^{l'\mu'n'}_{l\mu n}L^{j}_{t} = (2l+1)(2l'+1)\frac{1}{A^{j}N}\sum_{k=1}^{N} e^{-it\omega}\,\dot{T}^{*\mu n}_{l}(Q_A)\,\dot{T}^{*\mu'n'}_{l'}(Q_B)\delta_k \tag{3}$$

where N is the number of grain boundary segments seen on section j, δ_k is the length of the kth segment, and the asterisk (*) denotes the complex conjugate function. These coefficients are obtained for each section plane. Each set of coefficients is then used by section in determining the desired function, $f(Q_A, \mathbf{n}^{L}, Q_B)$.

A unique relationship exists between the coefficients $^{l'\mu'n'}_{l\mu n}L^{j}_{t}$ and $^{l'\mu'n'}_{l\mu n}S^{p}_{r}$, and is given by

$$^{l'\mu'n'}_{l\mu n}L^{j}_{t} = \frac{1}{\sqrt{2\pi}}\sum_{r=|t|}^{R}\sum_{p=-r}^{r} {}^{l'\mu'n'}_{l\mu n}S^{p}_{r}\,T^{tp}_{r}({}^{j}Q)\,I^{t}_{r} \tag{4}$$

which is an extension of results derived by Adams [19,20]. The solution to this set of linear complex equations yields the values of the $^{l'\mu'n'}_{l\mu n}S^{p}_{r}$ coefficients, allowing the estimation of $f(Q_A, \mathbf{n}^{L}, Q_B)$ as given in equation (2). R is the truncation value for the r index. As R goes to infinity, the resulting determination of the $^{l'\mu'n'}_{l\mu n}S^{p}_{r}$ coefficients becomes more precise. I^{t}_{r} are integration constants defined by

$$I^{t}_{r} = \int_{0}^{\pi} \bar{P}^{t}_{r}(\cos\nu)\,\sin^{2}\nu\,d\nu \tag{5}$$

where $\bar{P}^{t}_{r}(\cos\nu)$ are the associated Legendre polynomial functions.

The ${}^{l'\mu'n'}_{l\ \mu\ n}L^{j}_{t}$ coefficients, $T^{tp}_{r}({}^{j}Q)$ functions, and ${}^{l'\mu'n'}_{l\ \mu\ n}S^{p}_{r}$ coefficients are all complex; the I^{t}_{r} functions are real-valued. Solution of this equation requires consideration of the real and imaginary parts of the equations separately;

$$\mathrm{Re}({}^{l'\mu'n'}_{l\ \mu\ n}L^{j}_{t}) = \frac{1}{\sqrt{2\pi}}\sum_{r=|t|}^{R}\sum_{p=-r}^{r}\left[\mathrm{Re}({}^{l'\mu'n'}_{l\ \mu\ n}S^{p}_{r})\mathrm{Re}(T^{tp}_{r}({}^{j}Q)) - \mathrm{Im}({}^{l'\mu'n'}_{l\ \mu\ n}S^{p}_{r})\mathrm{Im}(T^{tp}_{r}({}^{j}Q))\right]I^{t}_{r} \tag{6}$$

and

$$\mathrm{Im}({}^{l'\mu'n'}_{l\ \mu\ n}L^{j}_{t}) = \frac{1}{\sqrt{2\pi}}\sum_{r=|t|}^{R}\sum_{p=-r}^{r}\left[\mathrm{Im}({}^{l'\mu'n'}_{l\ \mu\ n}S^{p}_{r})\mathrm{Re}(T^{tp}_{r}({}^{j}Q)) - \mathrm{Re}({}^{l'\mu'n'}_{l\ \mu\ n}S^{p}_{r})\mathrm{Im}(T^{tp}_{r}({}^{j}Q))\right]I^{t}_{r}. \tag{7}$$

Solving these equations is enabled by first setting t equal to the truncation order, R. There are four such equations obtained from each section plane because equations involving t and -t include the same two unknowns, $\mathrm{Re}({}^{l'\mu'n'}_{l\ \mu\ n}S^{p}_{r})$ and $\mathrm{Im}({}^{l'\mu'n'}_{l\ \mu\ n}S^{p}_{r})$, in the equations due to taking r=|t| in the summation. The maximum number of unknowns in these equations occurs for those coefficients which have r=R. For r=R, there are 2(2R+1) unknowns for which to be solved. Since four independent equations can be derived from each section plane, at least R+1 sections must be analyzed in order to obtain a unique solution to the system of equations described. Solving for the highest-order coefficients first allows substitution back into equations (6) and (7) for solution of the lower-order coefficients.

The system of equations described above is overdetermined by two equations for the required number of section planes, R+1. The best solution to these equations is found by the method of singular value decomposition, SVD [21,22]. The subroutine used in the SVD procedure for the present analysis is that listed in Numerical Recipes [21].

The damaged surface area per unit volume as a function of Q_A, $\mathbf{n}^L$, and Q_B, $f^D(Q_A, \mathbf{n}^L, Q_B)$, can be estimated by the same type of analysis described above. The data utilized in this calculation obtains from the damaged boundaries only. That is, the function ${}^{j}L^{D}_{A}(Q_A,\omega,Q_B)$ is found using equation (1). The number of grain boundary segments considered in the analysis, however, is the number which define grain boundary damage, and not the total number (see Experimental Details for explanation on separating the damaged and undamaged data). The analysis for determining $f^D(Q_A, \mathbf{n}^L, Q_B)$ follows precisely the procedure described above. The area fraction of damaged interface as a

function of the orientation parameters is subsequently determined as the quotient of $f(Q_A,\mathbf{n}^L,Q_B)$ and $f^D(Q_A,\mathbf{n}^L,Q_B)$:

$$S_S^D = \frac{\iiint_{Q,\mathbf{n},Q} f^D(Q_A,\mathbf{n}^L,Q_B)\, dQ_A\, d\mathbf{n}^L\, dQ_B}{\iiint_{Q,\mathbf{n},Q} f(Q_A,\mathbf{n}^L,Q_B)\, dQ_A\, d\mathbf{n}^L\, dQ_B} \tag{8}$$

where S_S^D is the surface area per unit surface, or area fraction, of damaged interface. Considering discrete points of $f^D(Q_A,\mathbf{n}^L,Q_B)$ and $f(Q_A,\mathbf{n}^L,Q_B)$ yields the area fraction of damaged interface as a function of interface normal orientation and crystallite lattice orientations, $S_S^D(Q_A,\mathbf{n}^L,Q_B)$.

It should be noted that the above discussion describes the procedure of determining the ${}^{l'\mu'n'}_{l\mu n}S_r^p$ (and ${}^{l'\mu'n'}_{l\mu n}L_t^j$) coefficients for only the largest domain of an IDF considered in this investigation. Similar procedures may be utilized in estimating the coefficients defining the functions with differing or reduced domains.

3. Experimental Details

Half-hard oxygen free electronic (OFE) alloy 101 copper plate (99.99% pure) with a thickness of 1.27 cm was machined into plane-strain tensile specimens with the dimensions shown in Figure 1. The region of gage section which experienced a stress-state of plane-strain tension was identified by photo-elastic techniques to be approximately the middle one-third of the specimen width. The stress was observed to be reasonably uniform through the thickness of the gage sections (height of 6.35 mm shown in Figure 1). The maximum tensile axis of each specimen was aligned with the rolling direction in the plate. The specimens were annealed at 900º C in a vacuum of 10^{-6} torr for two hours and subsequently furnace cooled. The resulting grain size was 169 μm (including twins as individual grains) with roughly equiaxed grains throughout the structure. Creep experiments in plain-strain tension with a Von Mises equivalent stress of 10 MPa were performed using dead-weight loading. The specimens were crept at 540º C (0.6 T_m) for 18 hours (≈ 0.6 t_r, where t_r is the time to rupture). After unloading, the specimens were again allowed to furnace cool. The axial strain measured from the creep tests was less than 2 percent, which indicates a maximum average strain-rate on the order of 3.0×10^{-8} s^{-1}.

To analyze and quantify the grain boundary damage, seven unique plane sections were cut through the gage sections of the specimens. The orientations of these sections are here defined in terms of Eulers angles. The sections used in the analysis with their corresponding Euler angles are given in Table 1. This set of test plane normal orientations covered the surface of the unit sphere with reasonable uniformity. Sectioning was performed using a spark cutter with care taken to minimize damage to the microstructure as the cuts were made. The depth of damage on the plane surfaces from use of the spark cutter is estimated at 1 μm. The cutting was followed by a slight electrochemical polish which removed all surface damage caused by the spark cutter and yet care was taken to not significantly effect the cavities observable on the plane section.

To collect the information needed in the analysis, the resulting structure of the copper specimens is digitized and subsequently analyzed with the aid of appropriate software. The structure is carefully scrutinized to determine the positions of the grain boundary segments and interface damage which is observable in the plane sections. This procedure requires significant experimental effort due partially to the fact that optical techniques are insufficient in accurately determining grain morphology, and therefore diffraction was utilized for grain map construction. Approximately 15 hours were required for the complete analysis of a small region on a plane section comprising some 150 grains. At least two such regions were examined for each of the seven test sections considered.

To digitize the microstructure, the plane section of the specimen is placed in a scanning electron microscope (SEM) with care taken to align a known specimen direction with the coordinates of the microscope (which becomes the reference coordinate frame). The SEM image of the section is subsequently captured on a computer equipped with an appropriate image card, and a map of the grain boundaries is constructed using the following procedure: The micrometer bar seen on the image is digitized by locating its end points with the cursor (this is needed for calibration purposes). The lower left-hand corner of the box to be digitized is located followed by the upper right-hand corner. The grain boundaries falling within this box are then digitized by locating the endpoints of line segments forming the boundaries. Two files are created for each section. The first file contains only the undamaged boundary segments and the second file contains only those which define the damaged portions of crystallite interface. Each line segment is defined by two pairs of x-y coordinates. Note that the first grain boundary point is the fifth point of each digitized file (because the first four points are needed to calibrate and define the dimensions of the box). It is important to remember that all grain boundaries are not readily visible on the screen and boundaries

should be located and verified using the electron back-scattered diffraction apparatus. Voids on the interfaces were defined as damage if they were apparent at a magnification of 1000x on the SEM.

The orientation of each individual crystallite was measured using the back-scattered electron diffraction method (analysis of back-scattered Kikuchi diffraction (BKD) patterns) [23,24]. A point within each grain corresponding to a given orientation was manually digitized in order to automatically correlate grain boundaries with the adjoining grains. The length and orientation of each line segment (representing a portion of a grain boundary) was determined by the computer and data files were generated which contained this information as well as the crystallite orientations of each grain comprising the interface. Reference [25] explains the experimental construction and interpretation of these grain maps in more detail along with a description of the software used in the analyses. The data set collected for this analysis included approximately 2200 individual lattice orientations measured with 8000 grain boundaries digitized. The stereological measure ${}^{j}L_A(Q_A, \omega, Q_B)$, as described in the previous section, was used in the analysis of the data and the determination of the IDFs. $f(Q_A, \mathbf{n}^L, Q_B)$ was determined from ${}^{j}L_A(Q_A, \omega, Q_B)$ via the fundamental equation of section analysis, equation (4). The seven section planes examined in this study restricts the maximum truncation order, R (as in equation 4), to six.

4. Results and Discussion

In the following sections the area fraction of damage is considered as a function of interface normal orientation, crystallite lattice misorientation, individual lattice orientations of crystallites composing the interface, and domains comprising various combinations of these variables. The complete IDF lies in an eight-dimensional orientation space. To investigate the character of this function, two-dimensional projections of the eight-dimensional domain have been analyzed in an attempt to identify the type of interfaces on which damage preferentially occurs. The parameters defining the maximum occurrence of damage seen in each of these projections is subsequently utilized in the determination of the damage distribution in an increased domain. For example, the area fraction of damage is estimated as a function of grain boundary normal orientation. From this function, the interface normal orientation of the maximum occurrence of damage is identified and then input as a constant for the IDF as a function

of lattice misorientation. This function becomes the area fraction of damaged interface with a given normal orientation, as a function of lattice misorientation.

4.1 Damage as a Function of Interface Normal Orientation

The first step taken to identify preferentially damaged boundaries was to find the interface normal orientation of the grain boundaries which were most readily damaged. The Fourier series expansion of ${}^{j}L_A(\omega)$ and $f(\mathbf{n}^L)$, analogous to those given in equations (1) and (2) are

$$ {}^{j}L_A(\omega) = \sum_{t=-\infty}^{\infty} L_t^j \, e^{it\omega} \tag{9} $$

and

$$ f(\mathbf{n}^L) = \sum_{r=0}^{\infty} \sum_{p=-r}^{r} S_r^p \, K_r^p(\mathbf{n}^L) . \tag{10} $$

The function $S_S^D(\mathbf{n}^L)$, calculated using these equations and their corresponding damaged portions, is represented in a stereographic projection over the unit sphere as seen in Figure 2. As expected, this distribution of damage differs markedly from that observed in the case of polycrystalline copper crept in uniaxial tension [15]. In the present study the boundaries oriented normal to the axis of loading, where the highest normal tensile stresses occurred, were the most preferentially damaged, with a 14 percent area fraction of damage. However, a significant area fraction of damage was also observed in the region where the polar angle (the angle from the normal, or unconstrained, direction) is approximately 80 degrees. In addition, there are several peaks near the axis of the constrained direction, which indicates the effect of the tensile stress arising from the constraint in that direction. For the case of uniaxial tension, the distribution of damage as a function of interface normal orientation consists of a single peak for the interfaces normal to the tensile direction, and a relatively uniform distribution of damage elsewhere [15]. From this result, one might conclude that, under the given conditions, the area fraction of damage is proportional to the magnitude of the applied tensile stress normal to the interface. For the case of plane-strain tension, however, this result is not entirely supported. Examination of Figure 2 reveals that the distribution of damage as a function of interface normal orientation is a function of more than just the magnitude of the applied tensile stress normal to the interface.

There are a number of factors, some of which may be of secondary importance, which possibly contribute to this result. The inhomogeneity of damage on interfaces of a given normal orientation suggests that local grain boundary structure, as well as non-local factors affect the propensity for a given interface to suffer damage. If the structure distribution of grain boundaries in the specimen is such that damage resistant interfaces are preferentially aligned in a given direction, the damaging effects of the normal stress across a boundary may be overcome. Assuming the statistics and measurements are reliable, the lack of a secondary peak aligned with the constrained direction, for example (which has a relatively high component of normal stress), may indicate a propensity for damage resistant boundaries to preferentially form in that direction as a result of thermo-mechanical processes.

4.2 Damage as a Function of Least Misorientation Angle

Damage was investigated as a function of least misorientation angle between adjoining crystallites, without regard to the axis of rotation. While this parameter does not describe the geometry of the interface, it is useful in a quick assessment of the data. This analysis was performed by counting all grain boundary segments making up the grain maps described in a previous section, without consideration of the segment lengths. The damaged segments were then counted separately, again without considering the lengths of the damaged segments or the fraction of damage. Figures 3.a and 3.b show the number of total boundaries and damaged boundaries as functions of misorientation angle.

The large number of boundaries with misorientation angle near 60º, seen in Figure 3.a, is indicative of the presence of many twin boundaries in the structure. In fcc materials the twin boundary is described by a 60º rotation about the [111] axis (Σ3 in CSL notation). The large number of twin boundaries in the structure is characteristic of annealed fcc materials with low stacking fault energies. Figure 3.b shows a large number of damaged boundaries with misorientation angle near 60º. We note that not all of these are twin boundaries. Damage was observed, however, on a number of grain boundaries exhibiting the Σ3 misorientation, but always off the coherent twin plane. This finding has been reported previously [28]. This is also consistent with McLean's energy calculations for the Σ3 boundary as a function of interface orientation, showing a definite minimum for the coherent (111) plane [29]. Figure 3.c shows the fraction of damaged boundaries as a function of misorientation angle. The damage fraction is given as a number fraction alone, without consideration of the area fraction of damage. Note that only a small fraction of the 60º boundaries are damaged even though the largest number

of damaged boundaries had misorientation angles near this value. The maximum fraction of damage as seen in Figure 3.c is 0.259 and occurs at a misorientation angle of 25º.

4.3 The Lattice Misorientation Dependence of Interface Damage

The function $S_S^D(\mathbf{n}^L, Q^c)$ was utilized in investigating damage as a function of lattice misorientation. The equations

$$ {}^{j}L_A(\omega, Q^c) = \sum_{t=-\infty}^{\infty} \sum_{l=0}^{\infty} \sum_{\mu=0}^{M(l)} \sum_{\nu=0}^{M(l)} {}_{l\mu\nu}L_t^j \, e^{it\omega} \, \ddot{\dot{T}}_l^{\mu\nu}(Q^c) \tag{11} $$

and

$$ f(\mathbf{n}^L, Q^c) = \sum_{r=0}^{\infty} \sum_{p=-r}^{r} \sum_{l=0}^{\infty} \sum_{\mu=0}^{M(l)} \sum_{\nu=0}^{M(l)} {}_{l\mu\nu}S_r^p \, K_r^p(\mathbf{n}^L) \, \ddot{\dot{T}}_l^{\mu\nu}(Q^c), \tag{12} $$

where $\ddot{\dot{T}}_l^{\mu\nu}(Q^c)$ are the generalized spherical harmonics possessing cubic-cubic symmetry, (as well as those equations describing the damaged interfaces) were employed to determine an IDF with functional dependence upon lattice misorientation and interface normal orientation. To isolate the boundaries which were most preferentially damaged, the interface normal orientation was fixed to be aligned with the rolling direction (the direction of maximum applied tensile stress), and the area fraction of damage was determined at discrete points over the asymmetric subspace of cubic-cubic misorientations as given by Zhao and Adams [30,31].

The measured interface structure distribution function (ISDF), $f(\mathbf{n}^L, Q^c)$ given by Adams [19], is essentially identical to that determined previously [15], with the major peak centered at the position of the Σ3 twin boundary (see Figure 4). A comparison of the area fractions of damage over this domain, however, reveals that the imposed stress-state significantly affects the character of the boundaries which are preferentially damaged. Figure 5 shows the function $S_S^D(\mathbf{n}^L, Q^c)$ plotted for a fixed value of $\mathbf{n}^L$ (aligned with the principal stress axis), and constant Φ sections. While several features of this IDF are similar to that calculated for uniaxial tension, the major peaks of the functions lie at differing misorientation values. The major peaks in the function for the case of uniaxial tension are at relatively low angles of misorientation. Figure 5 exhibits minor peaks near these values, but the major peaks in the function for the present analysis lie in

positions of high angle boundaries. These boundaries, however, lie on the boundary of the asymmetric domain similar to the previous analyses.

The lack of similarity between the IDFs calculated for specimens crept in uniaxial tension [15] and that of the present discussion suggests a strong stress-state dependence of damage over the space of lattice misorientations. In each IDF investigation of the inhomogeneity of creep damage, the boundaries observed to preferentially suffer damage tended to lie upon the border of the asymmetric region. This result strongly supports the previous conclusion that interfaces of a special geometrical construction are preferentially damaged and can be identified through the use of the IDF. It also suggests that stress-state plays an important role in determining the specific character of interfaces on which damage most readily occurs.

4.4 Damage as a Function of Individual Lattice Orientation

The domain of the IDF with dependence upon individual lattice orientations lies in an eight dimensional space. To investigate this space, the IDF as a function of interface normal orientation and a single crystallite orientation is first considered. The function $f(Q_A, \mathbf{n}^L, Q_B)$, given in equation (2), is integrated over the space of Q_B which retrieves $f(Q_A, \mathbf{n}^L)$, the desired function. The same integration is performed on the damaged parts of the function to enable the IDF determination in this domain. These were determined utilizing equation (2), with $\dot{T}_l^{\mu n}(Q)=1$ for l=μ=n=0, $\dot{T}_l^{\mu n}(Q)=0$ otherwise. Truncations of the series expansions were made at r = 6 and l = 16.

Figure 6 shows various projections of the function $S_S^D(Q_A, \mathbf{n}^L)$ (where $\mathbf{n}^L$ is constant) for the specimens crept in plane-strain tension. A plot of the IDF, over this domain, for specimens crept in uniaxial tension (which is given in a previous paper [15]), is presented in Figure 7 for the purpose of comparison. Certain features of the IDF from plane-strain tension specimens are similar to that determined from the specimens crept in uniaxial tension in this domain. The major peaks of these two functions, however, are quite different. This is best seen by a comparison of the contour plot at $\Phi = 70^\circ$; Figure 6 shows several steep peaks in this section, while Figure 7 exhibits very little damage on boundaries which border a crystallite orientation which maps into the region of $\Phi = 70^\circ$ for the uniaxially crept specimens. The stress-state dependence of the IDF is illustrated very well by this comparison. The slip systems which are active in a given crystallite depend upon its orientation relative to the given stress-state. It follows that by altering the stress-state the operative slip systems within a crystallite of a given orientation also change. This will, in turn, alter the local stress gradient at a grain boundary with normal

of a given orientation, thereby changing the expected distribution of damage on that interface. The maximum occurrence of damage determined in this domain is 0.404 for crystallites having orientation given by the Euler angles φ_1=50˚, Φ=80˚, and φ_2=40˚.

Expanding the analysis of the data to include all eight dimensions of grain boundary structure requires determination of the coefficients ${}^{l'\mu'n'}_{l\ \mu\ n}S^{p}_{r}$ seen in equation (2). The truncation of the series was made at r=6, *l*=8, and *l´*=8 to allow determination of the coefficients in a reasonable period of computing time. To identify severely damaged boundaries in this eight-dimensional space, the interface normal orientation was fixed, aligned with the tensile axis of the specimens. The orientation of the first crystallite was also held constant at φ_1=50˚, Φ=80˚, and φ_2=40˚ in order to correspond with the orientation exhibiting the maximum occurrence of damage as discussed in the previous paragraph. Recall that with the stereological measure ${}^{j}L_A(Q_A, \omega, Q_B)$, used in this analysis, it is possible to determine a "sided" function (see reference [15]). Therefore, it is important to understand that the interface normal is aligned with the "positive" rolling direction of the plate, as opposed to the "negative" rolling direction, and the orientation of the first crystallite is that which lies at the "tail" of the interface normal vector $\mathbf{n}^L$.

Figure 8 shows a series of projections of an IDF plotted in constant Φ sections of the neighboring crystallite orientation (the interface normal and first crystal lattice orientation are fixed at the maximum values determined above). The maximum value of the IDF calculated in this space was 0.595 at an orientation of Q_B=(90,70,70). This orientation lies at a misorientation angle of 36.4˚ from the neighboring crystallite which is not a position of maximum damage as a function of least misorientation angle, seen on Figure 3.c. The misorientation of this pair of crystallites maps near the boundary of the asymmetric domain of cubic-cubic misorientations in Euler space at Q^c=(37,77,44) which lies near a peak of 0.534 on the damage plot shown in Figure 5. The group multiplicity of misorientations which lie on this face of the asymmetric subspace is two The particular misorientation listed above is within one degree of satisfying Brandon's criterion [30] for being classified as a Σ3 CSL boundary. A listing of various major peaks from Figure 8, their misorientations from the neighboring crystallite, and group multiplicities is found in Table 2. While none of these boundaries satisfies the criterion of "specialness" as defined by CSL theory, they are generally centered on regions with multiplicity in misorientation space greater than one. This supports our previous observation that boundaries having misorientations which lie on the boundary of the asymmetric domain in Euler space are preferentially damaged. Deriving this conclusion from systematic analysis of interface structure in eight-dimensional space, subsequent to

arriving at the same conclusion by analysis of misorientation space, lends credence to the analytical methods employed.

5. Speculation on Microstructural Mechanisms

Various researchers have concentrated on isolating microscopic damage mechanisms [cf. 33,34]. Fracture mechanism maps which show the suspected dominating mechanism as a function of stress and temperature have been constructed for a number of materials [35,36]. Ashby and his co-workers identify the primary mechanisms as volume diffusion (Nabarro-Herring creep [37,38]), surface diffusion (Coble creep [39]), and dislocation mechanisms which cause creep behavior to have a power law dependence. These maps are generally useful in predicting fracture life of a component but do not consider the heterogeneity of damage in the microstructure and are therefore used only as a first step in isolating mechanisms. In this section we discuss a number of mechanisms which may be responsible for damaging polycrystalline interfaces, and factors which contribute to damage heterogeneity.

It has long been theorized that grain boundary voids can grow by diffusion of atoms away from the surface of a void or nucleus [6,7]. The growth of the voids is dependent upon the stress imposed on the boundary. Local stress gradients in a polycrystal are a function of several variables, one of which is the structure of crystallite interfaces. Grain boundaries on which high stresses are present may be more readily damaged by diffusion, grain boundary sliding, or by some other mechanism. It has been shown that boundaries which experience a large tensile hydrostatic component of stress suffer greater damage than those on which the hydrostatic pressure is negligible or compressive [6,40]. While several models exist to calculate the local stress gradient at a point in a polycrystal (cf. [41,42]), there is never enough available information on the microstructure of the material to find the stress gradient with high certainty.

5.1 Group Multiplicities, Low Interface Energy, and Intergranular Damage

It is difficult to determine the physical mechanisms which cause interfaces with certain "special" types of misorientations to preferentially damage. The energy and structure of an interface is unknown because the crystallographic planes which form the boundary are not given. Even when this information is known, as in the case of the eight-dimensional IDFs, the structure and energies can be reliably estimated for only the simplest situations. It has been remarked that grain boundary structure and energy are

not uniquely related to misorientations, and that CSL and other theories should not be used to predict atomic structure or energy of crystallite interfaces [13].

A conclusion which has been consistent in the present work and our previous work in the uniaxial tensile stress state is that some interfaces which exhibit a group multiplicity greater than one are preferentially damaged. Group multiplicity in this sense defines the number of physically indistinguishable misorientations. One over the group multiplicity is the fraction of indistinguishable positions in comparison to the number of symmetry elements in the point group. Consider, for example, the point group of cubic-cubic symmetry. There are 24x24, or 576, misorientations which rotate the positions of the two lattices into physically indistinguishable positions. A misorientation which has a group multiplicity of two reduces this number by one-half, leaving 288 unique, physically indistinguishable misorientations when operated upon by the point group of cubic-cubic symmetry. This reduction of symmetry elements results from a partial overlap of the local symmetry groups of the two adjacent crystallites. The maximum multiplicity is 48 for the $\Sigma 1$ boundary (when misorientation is the identity). Random high-angle boundaries with no particular distinguishing features exhibit a multiplicity of one.

To investigate why these special boundaries are readily damaged, a projection of the eight-dimensional IDF from Section 4 showing boundary normal dependence with fixed crystallite orientations was determined. The orientations fixed are those from Figure 8 which suffered the maximum damage; $Q_A=(50^\circ,80^\circ,40^\circ)$ and $Q_B=(90^\circ,70^\circ,70^\circ)$. Recall that the misorientation of this boundary lies at $Q^c=(37,77,45)$ which lies on the boundary of the asymmetric subspace and exhibits a misorientation of two. This misorientation does not satisfy Brandon's criterion for specialness [32], but comes closest to satisfying the criterion of the $\Sigma 3$ boundary (group multiplicity is 12). This misorientation, in fact, lies within less than one degree of being classified as a $\Sigma 3$ boundary by this method. The determination of the IDF was made at distinct points on a 10°x10°x10° grid over the space of individual lattice orientations. It follows that misorientations which may be classified as $\Sigma 3$ boundaries lie near this peak of boundaries which are preferentially damaged as determined by the IDF. For the sake of argument, consider the peak in the function shown in Figure 8 to be a $\Sigma 3$ boundary. Figures 9.a and 9.b show the IDF plotted over the space of interface normal orientations for the given crystallite orientations. The box indicates the (111) plane in the crystallite given by $Q_A=(50,80,40)$ which corresponds to the coherent twin plane, (assuming that the misorientation between the lattices is a $\Sigma 3$ boundary). Notice that there is little or no damage indicated by the function in the position of the coherent plane.

Brandon, *et al.* [43] theorized that a high planar density of coincidence sites corresponds to low interfacial energy. A simple extension of this idea is used to investigate the preferentially damaged boundary discussed above. Assume that a high planar density of atoms, coincident or not, forms interfaces with relatively low energies and correspondingly low damage distributions. Consider two interpenetrating fcc lattices each centered about a given coincident atom. The first lattice has orientation Q_A=(50,80,40) and the second lattice orientation is given by the triplet Q_B=(90,70,70) (corresponding to the boundary investigated in Section 4 and the maximum peak seen in Figure 8). Consider a circular disk of a given radius and thickness which is centered about the aforementioned coincident atom (for this calculation the radius is 16 and the width is 2.5 lattice spacings). Let the normal to the plane surface of this disk have some orientation represented by a point in the stereographic projection of the unit sphere. For each normal orientation considered, determine the number of lattice points from each lattice which falls within this disk. This number divided by the volume of the disk defines the relative density of lattice points as a function of normal orientation. Figures 10.a and 10.b show the density of points for each lattice orientation, and Figure 10.c shows the density of points for the interpenetrating lattices. The values indicated on the contours are the density ratios of the given orientation to the volume average density. Notice the high density of lattice points on the (111) planes and the relatively low density on the (100) planes. The position of the coherent (111) twin boundary is clearly seen from Figure 10.c, where the highest density of points of the interpenetrating lattices occurs.

A qualitative comparison of Figure 9.a with Figure 10.c reveals an apparent dependence of intergranular creep damage on the planar density of atoms which form the interface. This result offers a possible explanation to the finding that certain special types of misorientations are preferentially damaged. These special boundaries contain a certain number of crystallographic planes which coincide, as in the case of the $\Sigma 3$ boundary, or which share a given density of coincident sites. The shared coincident sites may increase the density of atoms near an interface of similar normal orientation as the crystallographic planes of high coincidence. On the off-coincidence planes, however, the density of atoms near a planar interface correspondingly decreases. The boundaries which have a lower density of atoms near the interface are apparently preferentially damaged, depending on the stress relative to the interface normal orientation.

5.2 Slip Incompatibilities and Interface Segregation

Slip incompatibilities at an interface have been shown to be a cause of premature fracture in crept bicrystals [cf. 44]. If slip is not easily transferred across an interface, stress concentrations develop which may contribute to damage on the boundary. There are several models which predict slip transfer from a slip system in one crystallite to a particular slip system in an adjoining crystallite of given lattice orientation. The majority of these predict bicrystal type behavior and do not consider multiple active slip systems in each crystallite. A few of these models, and how they relate to the measured damage functions discussed previously, are given in the following paragraphs.

Among the earliest researchers to investigate the problem of slip transfer across an interface were Livingston and Chalmers [45]. In their bicrystal-type model of slip transfer they defined a slip transmission factor, N_{ij}

$$N_{ij} = (\mathbf{n}_i \cdot \mathbf{n}_j)(\mathbf{b}_i \cdot \mathbf{b}_j) + (\mathbf{n}_i \cdot \mathbf{b}_j)(\mathbf{b}_i \cdot \mathbf{n}_j) \tag{13}$$

where the indices i and j indicate slip system numbers. (i and j go from 1 to twelve for fcc materials). The larger the value of the transmission factor, the easier it is for slip system j in the first crystallite to be activated by slip system i in the adjoining grain. The maximum value of N_{ij} is one for compatible slip systems.

Shen, et. al. [46] have defined an additional criterion for slip transfer which incorporates the dependence of the interface normal orientation. Consider a unit vector, **l**, which defines the direction of the line of intersection of the slip plane in the grain boundary plane. The angles between lines of intersection of the slip planes with the grain boundary, and the slip directions are minimized. This can be expressed by

$$M = (\mathbf{l}_i \cdot \mathbf{l}_j)(\mathbf{b}_i \cdot \mathbf{b}_j) \tag{14}$$

where M must be maximized to define the slip system j activated by an adjoining grain with an operating slip system i.

A simple polycrystalline model for slip transfer which includes the assumption that several slip systems may be operating simultaneously was given recently by Werner and Prantl [47]. In this model, a slip transfer number, λ, is defined as

$$\lambda = \sum_{i=1}^{N^2} \left[\cos \frac{90°}{\varepsilon_c} \varepsilon_i \cos \frac{90°}{\kappa_c} \kappa_i \right]. \tag{15}$$

where N is the number of possible slip systems in the structure (eg. $N^2 = 144$ for fcc structures). ε is the angle between slip directions, and κ is the angle between the lines formed by the slip plane intersection with the grain boundary. The values ε_c and κ_c are the critical values of these angles (for fcc materials, the values $\varepsilon_c = 15^\circ$ and $\kappa_c = 45^\circ$ are assumed). The sum is performed only for those values of ε_i and κ_i which are less than or equal to the critical values. The larger the value of λ, the easier it is for slip to be transferred. If slip incompatibility is a determining factor as to the types of boundaries which are easily damaged, interface structures with low values of λ should correspond to those with a high area fraction of damage.

There have been a number of additional attempts to predict the crystallographic plane and direction on which a transmitted dislocation is likely to travel [12,48,49]. Most of these concentrate primarily on the assumption that a single slip system is operating in each crystallite. It is pointed out that slip may occur on planes which are not close packed. More specifically, aluminum, copper, and most fcc metals have been observed to glide on (110), (100), and (112) planes at sufficiently high temperatures [cf. 12]. The criteria used to determine slip planes and directions of transmitted slip, taking into consideration anomalous slip is similar to that described above. Additional criteria may be considered which includes maximizing shear stress and minimizing the magnitudes of Burgers vectors of the residual DSC dislocations at the interface [49].

Each of the models described above has been compared with the measured IDFs to determine whether interfaces which are predicted to have high slip incompatibilities correspond with those on which damage was observed to preferentially occur. While damage on certain boundaries corresponded with one model or another, none of the models satisfactorily offered conclusive evidence of slip incompatibility affects on intergranular creep damage.

Inhomogeneous chemical composition of polycrystalline interfaces is another cause of damage heterogeneity [50]. Solute segregation is an important factor in intergranular creep damage [51,52]. This may be related to interface geometry, however, in that the heterogeneity of segregation is dependent upon the structure of the grain boundary and, in fact, solutes at the interface may change the dislocation structure of the boundary [52]. An attempt was made at determining interfacial impurities in crept specimens. Utilization of energy-dispersive and wave length-dispersive x-ray analysis (EDX and WDX) techniques could not conclusively detect impurities on fracture surfaces. No differences in impurity content were observed between the fracture surfaces of crept and uncrept specimens. This offers no evidence, however, whether or not impurity elements had segregated to grain boundaries during creep since the interaction depth of the

electron beam is on the order of 0.25 μm, and impurity elements may cover a depth of only several angstroms.

6. Conclusions

Intergranular creep damage in specimens crept in plane-strain tension exhibited significant heterogeneity in the distribution of damage as demonstrated by the interface damage function. In general, significant damage occurs over a wider range of interface normal orientations than was observed in specimens crept in uniaxial tension [15]. Interfaces normal to the axis of maximum tensile stress suffered the largest fraction of damage while significant damage occurred on interfaces nearly normal to the axis of constraint.

The crystallite lattice misorientation dependence of damage differed significantly for the specimens crept in plane-strain tension from the results obtained previously [15]. Consistent with the previous IDF determinations, however, the group multiplicity of misorientations which are preferentially damaged tend to be greater than one. These misorientations map onto the boundary of the asymmetric subspace of cubic-cubic misorientations. The tendency of some of these boundaries to preferentially damage has been shown in previous IDF measurements [14,15].

The investigation of damage in specimens crept in plane-strain tension has again demonstrated the importance of individual lattice orientations in the determination of interfaces which are preferentially damaged. The amount of deformation and lattice rotation in a single crystallite depends upon its individual lattice orientation as well as upon the properties of the neighborhood in which it lies. To better understand the mechanisms of void growth it is important to include as much information as possible for use in various models predicting damage behavior. Those explicitly discussed in Section 5 utilize the eight parameter information obtained in the measured IDFs. Future models may require even more substantial information on the character of the microstructure, including some non-local information.

The heterogeneity of damage over the eight-dimensional space investigated shows that all three physical parameters defining interface geometry are useful in describing the occurrence of damage in polycrystalline materials. This is more convincingly demonstrated by comparing projections of the measured damage function against certain models which predict damage behavior. These models, such as slip incompatibility and

atomic planar density along crystallite interfaces, require all eight variables of the IDF as parameters in predicting behavior of the interface.

This paper, as well as previous studies [14,15], have demonstrated the utility of IDFs in analyzing the heterogeneity of intergranular damage. The obvious shortcoming of this method has been the inability to rapidly obtain large sets of data to ensure statistical reliability. Approximately 400 hours of experimental effort were required to obtain the data set used in this analysis (about 8000 grain boundaries). Recent developments will, it seems, make feasible the automatic analysis of grain boundary structure in future work. Following the procedures described in this paper, along with automatic collection of data, greater understanding of the physical mechanisms of damage heterogeneity is made possible. This may, in turn, lead to the development of more damage resistant polycrystalline materials.

Acknowledgement

The authors wish to acknowledge support of this work by the Office of Basic Energy Sciences of the U. S. Department of Energy.

References

1. J.B. Dennison and B. Wilshire: *J. Inst. Metals*, 1963, vol. 92, p. 343-360.
2. W.J. Evans and B. Wilshire: *Metall. Trans.*, 1970, vol. 1, p. 2133-2139.
3. N.G. Needham, J.E. Wheatley and G.W. Greenwood: *Acta Metall.*, 1975, vol. 23, p. 23-27.
4. I-W. Chen and A.S. Argon: *Acta Metall.*, 1981, vol. 29, p. 1321-1333.
5. B.F. Dyson, M.S. Loveday and M.J. Rodgers: *Proc. R. Soc. Lond. A*, 1976, vol 349A, p. 245-259.
6. D. Hull and D.E. Rimmer: *Phil. Mag.*, 1959, vol. 4, p. 673-687.
7. M.V. Speight and J.E. Harris: *Metal Sci.*, 1967, vol. 1, p. 83-89.
8. B.F. Dyson: *Metal Sci.*, 1976, vol. 20, p. 349-353.
9. J.R. Rice: *Acta Metall.,* 1981, vol. 29, p. 675-681.
10 J. Don and S. Majumdar: *Acta Metall.*, 1986, vol. 34, p. 961-967.
11. T. Watanabe: *Matls. Sci. Forum*, 1989, vol. 46, p. 25-48.
12. J. Bonneville, D. Caillard, M. Carrard and J.L. Martin: *Rev. Phys. Appl.*, 1988, vol. 23, p. 461-473.

13. V. Vitek, A.P. Sutton, D.A. Smith, and R.C. Pond in *Grain-Boundary Structure and Kinetics*, ASM Materials Science Seminar, Milwaukee, 1979, p. 115-144.
14. B. L. Adams, J. Zhao and D. O'Hara: *Acta metall. mater.*, 1990, vol. 38, p. 953-966.
15. D.P. Field and B.L. Adams: *Acta metall. mater.*, In Press.
16. R.H. Wagonner: *Metall. Trans.*, 1980, vol. 11A, p. 165-175.
17. B.L. Adams and D.P. Field: unpublished research, 1991.
18. H.J. Bunge: *Texture Analysis in Materials Science*, Butterworths, London, 1982, p. 353-403.
19. B. L. Adams: *Metall. Trans.*, 1986, vol. 17A, p. 2199-2207.
20. J. Zhao, J. S. Koontz and B. L. Adams: *Metall. Trans.*, 1988, vol. 19A, p. 1179-1185.
21. W.H. Press, B.P. Flannery, S.A. Teukolsky, and W.T. Vetterling: *Numerical Recipes*, Cambridge University Press, NY, 1986, p. 52-64.
22. G.H. Golub and C.F. Van Loan: *Matrix Computations*, Johns Hopkins University Press, Baltimore, 1983, Ch. 12.
23. J. A. Venables and C. J. Harland: *Phil. Mag.*, 1973, vol. 27, p. 1193-1200.
24. D. J. Dingley and K. Baba-Kishi: *Scanning Electron Microscopy*, 1986, vol. II, p. 383-391.
25. D.P. Field: PhD Dissertation, Yale University, 1991, p. 121-188.
26. D.C. Handscomb: *Can. J. Math.*, 1958, vol. 10, p. 85-88.
27. J.K. Mackenzie: *Biometrika*, 1958, vol. 45, p. 229-240.
28. A. Rukwied: *Metall. Trans.*, 1972, vol. 3, p. 3009-3023.
29. M. McLean: *J. mater. Sci.*, 1973, vol. 8, p. 571-576.
30. J. Zhao and B. L. Adams: *Acta cryst.*, 1988, vol. A44, p. 326-336.
31. B.L. Adams, J. Zhao and H Grimmer: *Acta cryst.*, 1990, vol. A46, p. 620-622.
32. D.G. Brandon: *Acta metall.*, 1966, vol. 14, p. 1479-1484.
33. A.S. Argon: *Recent Advances in Creep and Fracture of Engineering Materials and Structures*, B. Wilshire and D.R.J. Owens (Eds.), Pineridge Press, Swansea U.K., 1982, p.1-28.
34. R. W. Evans and B. Wilshire: *Creep of Metals and Alloys*, Pineridge Press, Swansea, 1985, p. 167-174.
35. M.F. Ashby, C. Gandhi, and D.M.R. Taplin: *Acta Metall.*, 1979, vol. 27, p. 699-729.
36. H.J. Frost and M.F. Ashby: *Deformation Mechanism Maps*, Pergamon Press, Oxford, 1982.

37. F.R.N. Nabarro: *Report of Conference on Strength of Solids*, Phys. Soc. of London, 1948, p.75-82.
38. C. Herring: *J. Appl. Phys.*, 1950, vol. 21, p. 437-443.
39. R.L. Coble: *J. Appl. Phys.*, 1963, vol. 34, p. 1679-1682.
40. A. C. F. Cocks and M. F. Ashby: *Prog. in Mat. Sci.*, 1982, vol. 27, p. 189-244.
41. B.L. Adams, G.R. Canova and A. Molinari: *Textures and Microstructures*, 1989, vol. 11, p. 57-71.
42. B.L. Adams and D.P. Field: *Acta metall. mater.*, 1991, vol. 39, p. 2405-2417.
43. D.G. Brandon, B. Ralph, S. Ranganathan and M.S. Wald: *Acta metall.*, 1964, vol. 12, p. 813-821.
44. R. Raj: *Acta metall.*, 1978, vol. 26, p. 341-349.
45. J.D. Livingston and B. Chalmers: *Acta metall.*, 1957, vol. 5, p. 322-327.
46. Z. Shen, R.H. Wagoner, and W.A.T. Clark: *Acta metall.*, 1988, vol. 36, p. 3231-3242.
47. E. Werner and W. Prantl: *Acta metall. mater.*, 1990, vol. 38, p. 533-537.
48. D.J. Dingley and R.C. Pond: *Acta metall.*, 1979, vol. 27, p. 667-682.
49. T.C. Lee, I.M. Robertson, and H.K. Birnbaum: *Metall. Trans.*, 1990, vol. 21A, p. 2437-2447.
50. S.P. Lynch: *Materials Science Forum*, 1989, vol. 46, p. 1-24.
51. E.D. Hondros and P.J. Henderson: *Metall. Trans.*, 1983, vol. 14A, p. 521-530.
52. K.E. Sickafus and S.L. Sass: *Acta metall.,* 1987, vol. 35, p. 69-80.

Figures and Tables

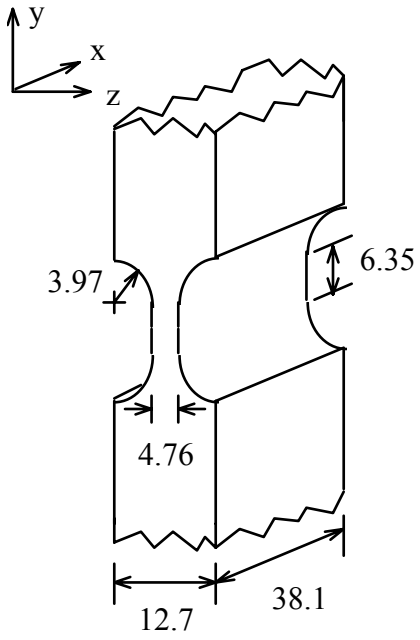

Figure 1 - Schematic of the plane-strain tensile specimen employed in the investigation.

Table 1 - Euler angles rotating the specimen coordinate frame into the jth section coordinate frame.

Section	φ_1	Φ	φ_2
1	75°	90°	0°
2	140	70	0
3	0	0	0
4	0	90	180
5	140	110	0
6	40	110	0
7	230	110	180

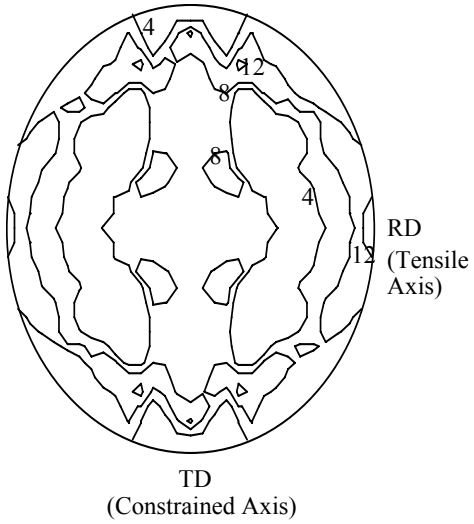

Figure 2 - IDF as a function of interface normal orientation. The contour lines are at 4, 8, and 12 percent damage.

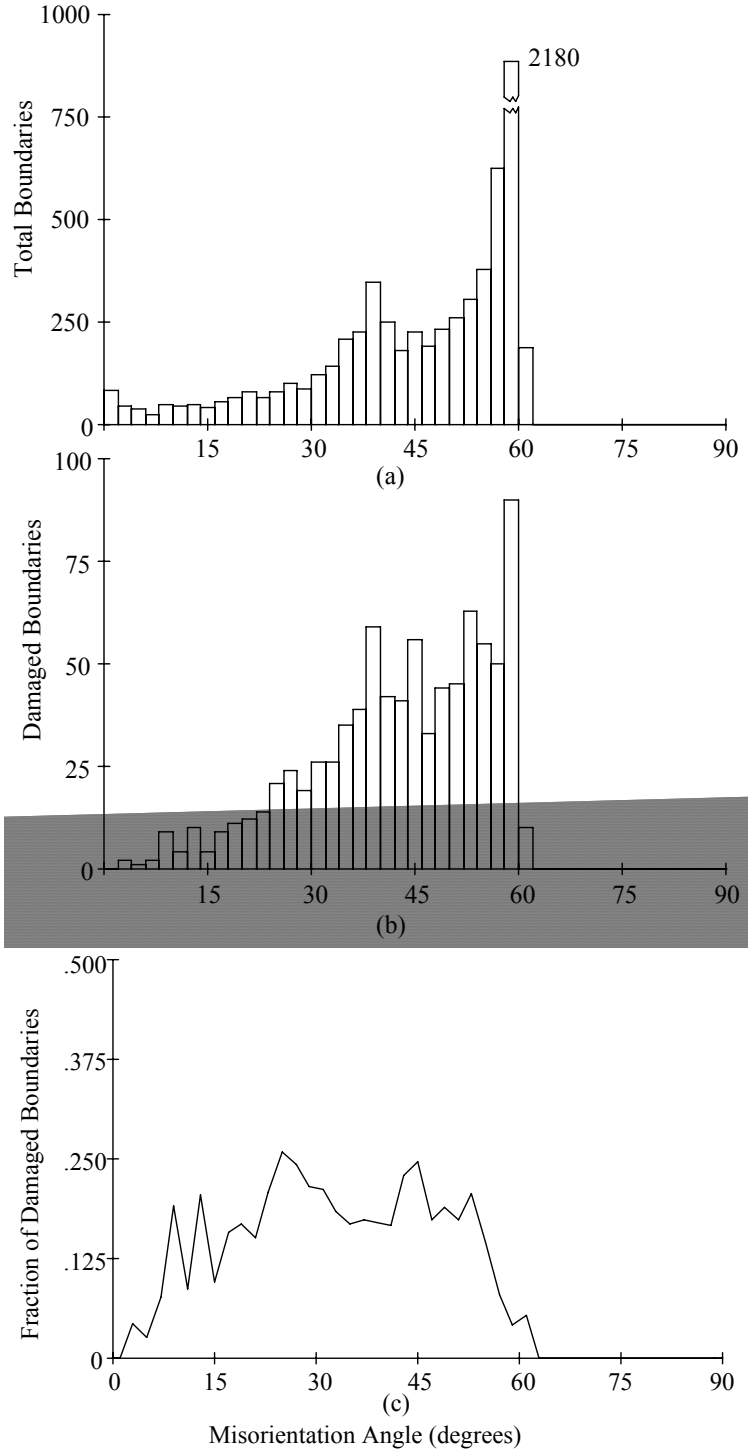

Figure 3 - (a) Total Boundaries, (b) Damaged Boundaries, and (c) Damaged fraction of grain boundaries as a function of least misorientation angle for plane-strain tension.

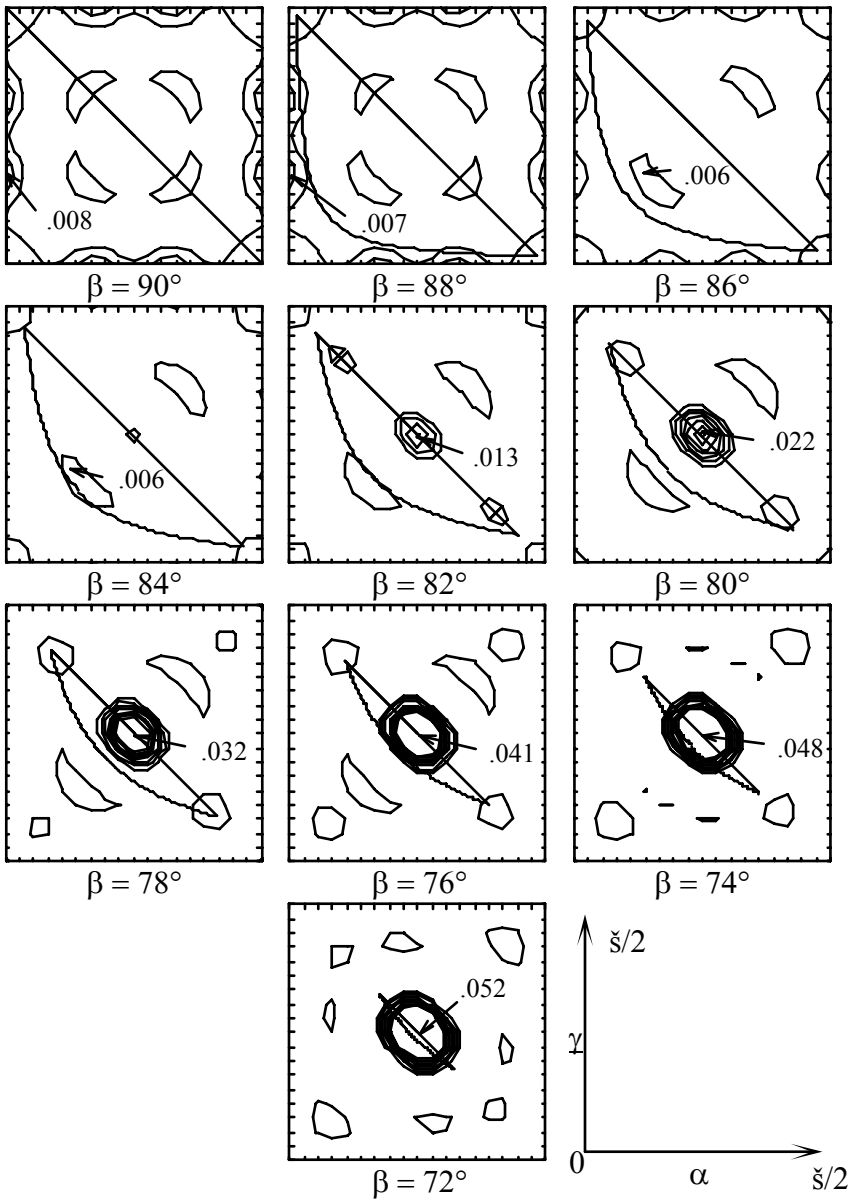

Figure 4 - f(90,90,Q^c), contour lines are at equal intervals of 0.3×10^{-3}/mm. Maximum peaks shown are x10/mm. The superimposed region shows the asymmetric subspace of cubic-cubic misorientations.

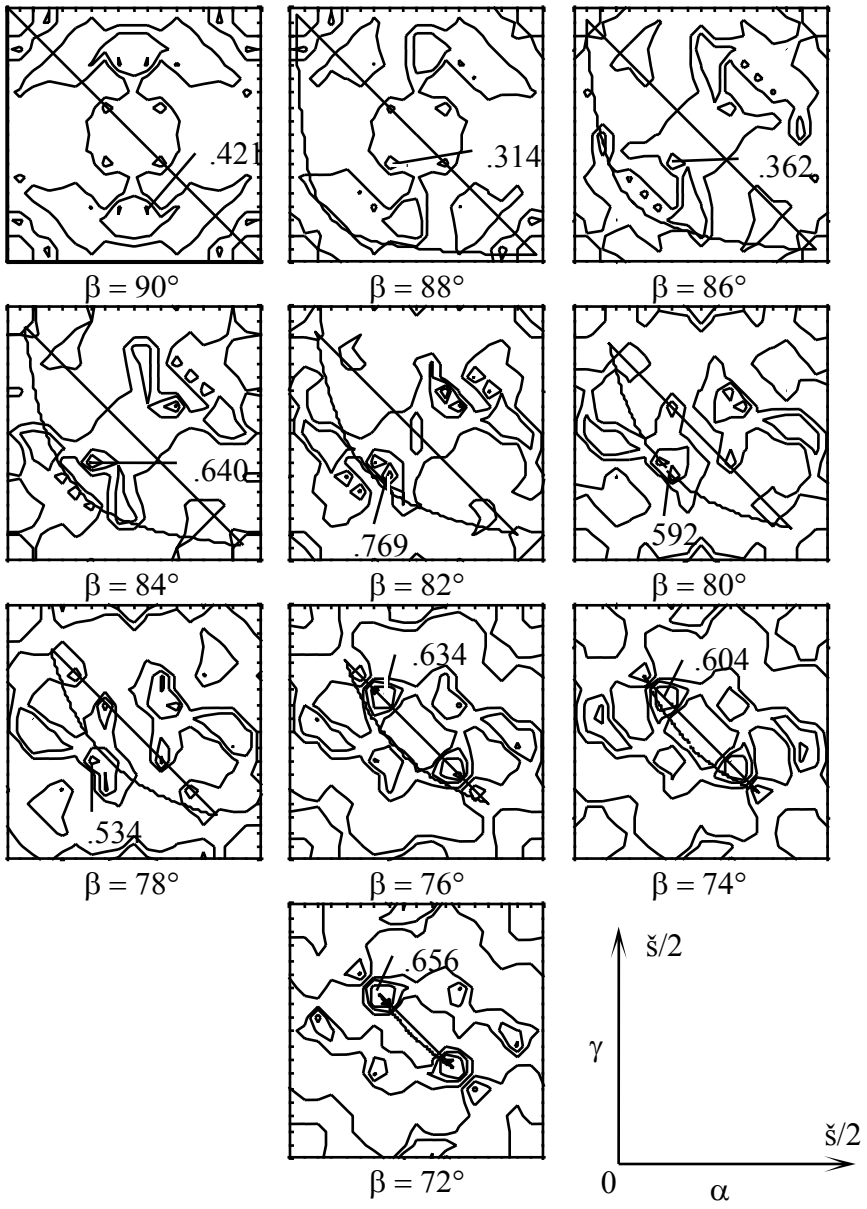

Figure 5 - IDF as a function of lattice misorientation. The interface normal orientation is aligned with the maximum applied tensile stress. Contours are at 0, 20, 40, and 60 percent damage.

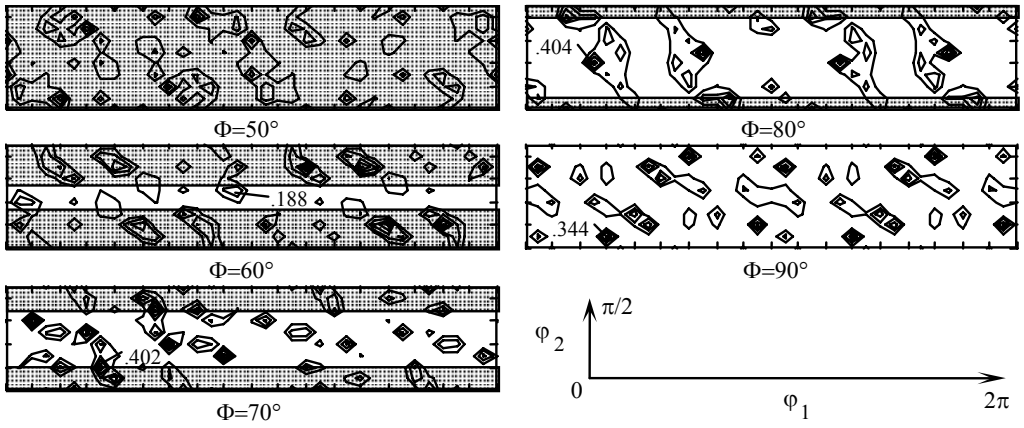

Figure 6 - IDF as a function of lattice orientation of a single crystallite with interface normals aligned with the maximum tensile stress axis for specimens crept in plane-strain tension. Contours are at 0, 10, 20, 30, and 40 percent damage.

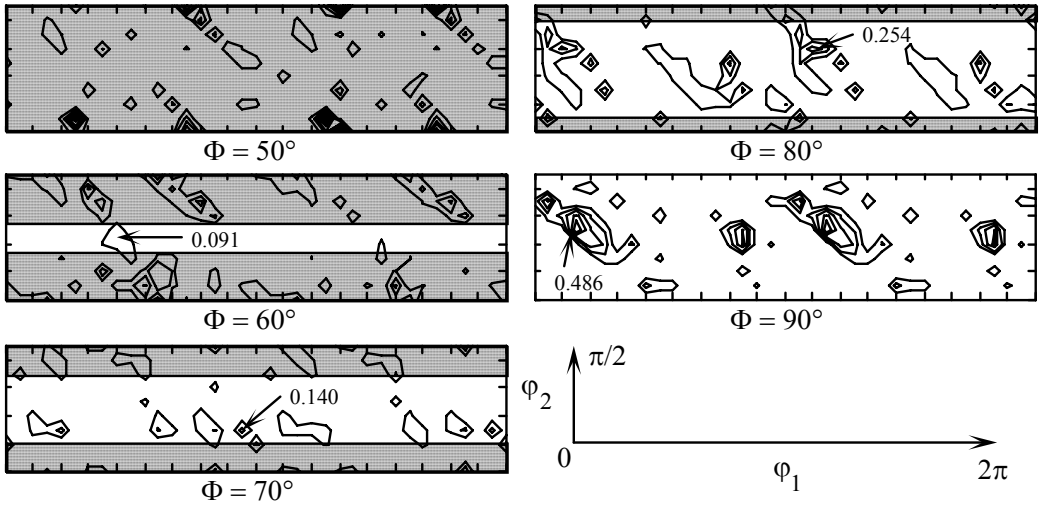

Figure 7 - IDF over the space of a single crystallite orientation for uniaxial tension. Maximum peak at Q_A=(30,90,50).

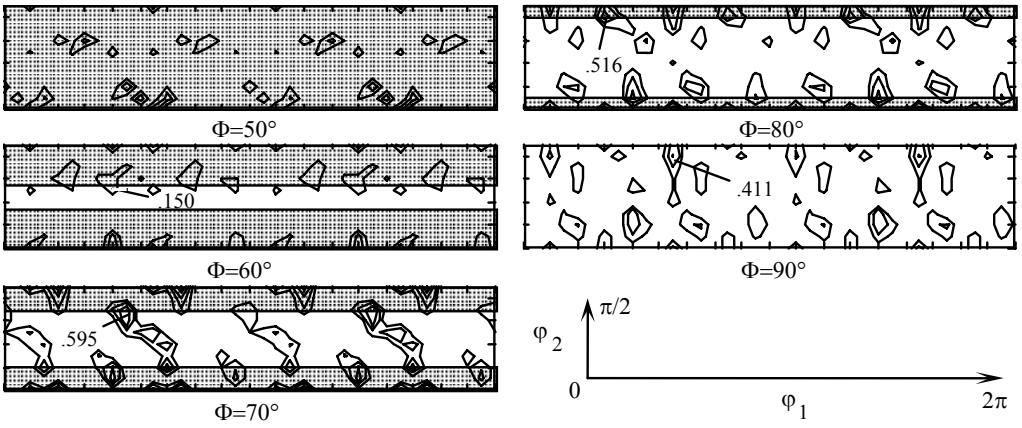

Figure 8 - IDF as a function of neighboring lattice orientation. Interface normal is aligned with the tensile axis and the orientation of the crystallite at the "tail" of the normal vector is g=(50,80,40). Contours are at 0, 20, and 40 percent damage.

Table 2 - Various peaks in the IDF over the space of the neighboring grain orientation for $\mathbf{n}^L$=(90,90), and Q_A=(50,80,40) (compare with Figure 8), along with their misorientations and group multiplicities.

Euler Angles of Adjoining Grain (Q_B) φ_1, Φ, φ_2	Calculated Damage Fraction	Euler Angles Defining Misorientation (Q^c) α, β, γ	Group Multiplicity of Misorientation
90, 70, 70	0.595	37, 77, 44	2
60, 80, 80	0.516	10, 88, 48	2
120, 70, 20	0.501	22, 78, 61	2
80, 80, 10	0.487	27, 84, 62	2
110, 90, 80	0.411	29, 89, 45	1

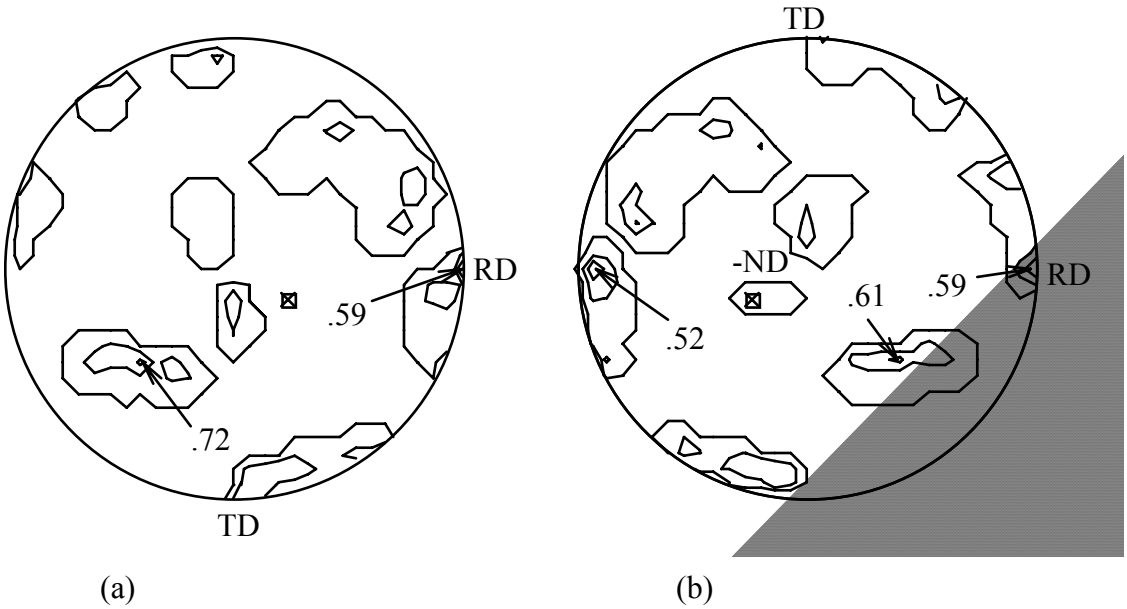

(a) (b)

Figure 9 - Fraction of damage for the lattice orientations Q_A=(50,80,40) and Q_B=(90,70,70) plotted over the space of interface normal orientation for (a) the positive normal direction, and (b) the negative normal direction. The box shows the position of the coherent twin plane, assuming that the orientations form a Σ3 boundary.

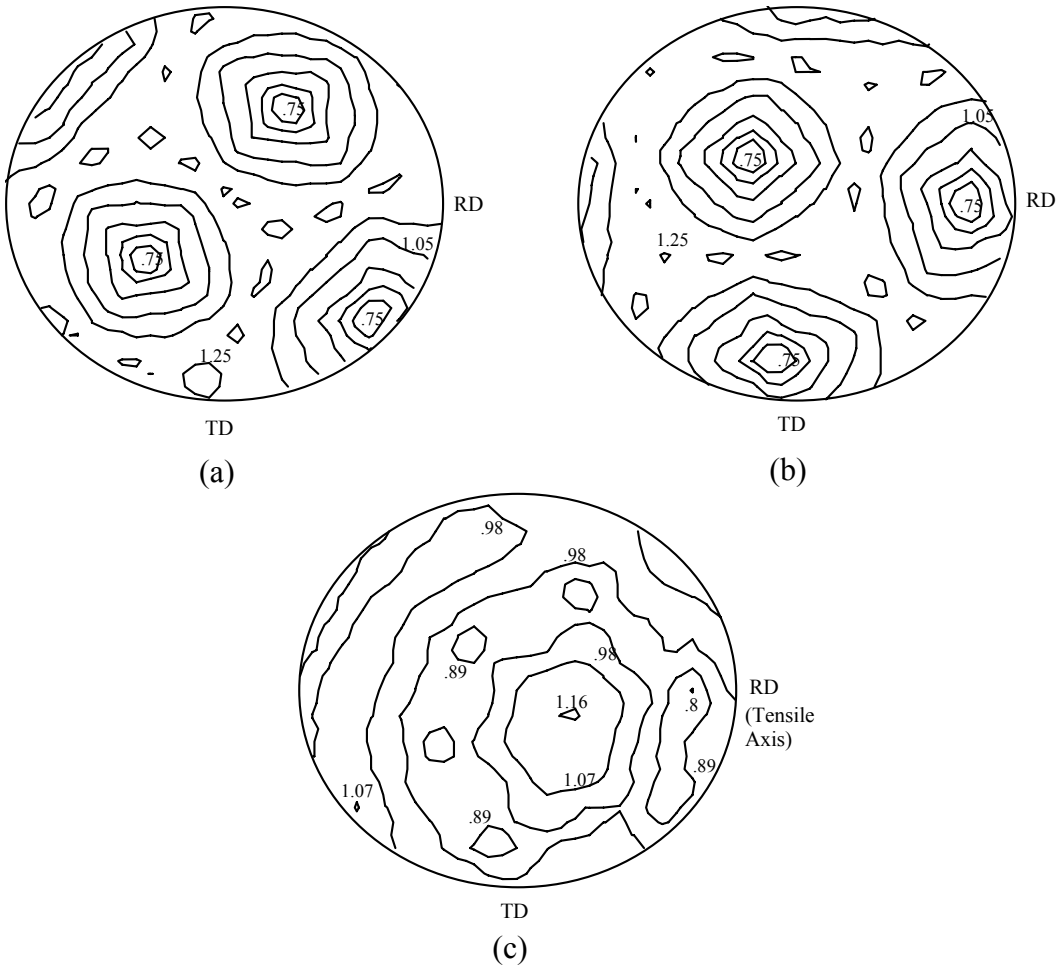

Figure 10 - The density of lattice points as a function of sampling plane normal orientation for (a) lattice of orientation Q_A=(50,80,40), (b) lattice orientation of Q_B= (90,70,70), and (c) the interpenetrating lattices.